Erosion of upland hillslope soil organic carbon: Coupling field measurements with a sediment transport model

Kyungsoo Yoo and Ronald Amundson
Division of Ecosystem Sciences, University of California, Berkeley, California, USA

Arjun M. Heimsath
Department of Earth Sciences, Dartmouth College, Hanover, New Hampshire, USA

William E. Dietrich
Department of Earth and Planetary Science, University of California, Berkeley, California, USA

Received 29 March 2004; revised 30 March 2005; accepted 10 May 2005; published 9 July 2005.

[1] Little is known about the role of vegetated hillslope sediment transport in the soil C cycle and soil-atmosphere C exchange. We combined a hillslope sediment transport model with empirical soil C measurements to quantify the erosion and temporal storage of soil organic carbon (SOC) within two grasslands in central California. The sites have contrasting erosional mechanisms: biological perturbation (Tennessee Valley (TV)) versus clay-rich soil creep (Black Diamond (BD)). The average SOC erosion rates from convex slopes were 1.4–2.7 g C m^{-2} yr^{-1} at TV and 5–8 g C m^{-2} yr^{-1} at BD, values that are <10% of above ground net primary productivity (ANPP) at both sites. The eroded soil accumulates on depositional slopes. The long term SOC accumulation (or C sink) rates are ~1.9 g C m^{-2} yr^{-1} in the TV hollow and 1.7–2.8 g C m^{-2} yr^{-1} in the BD footslope. We found that the hillslope C sink is driven primarily by the burial of in situ plant production rather than preservation of eroded SOC, a finding that differs from existing hypotheses. At TV, the net sequestration of atmospheric C by long-term hollow evacuation and refilling depends on the fate of the C exported from the zero order watershed. This study suggests that erosion and deposition are coupled processes that create a previously unrecognized C sink in undisturbed upland watersheds, with a potential to substantially affect the global C balance presently, and over geological timescales.

Citation: Yoo, K., R. Amundson, A. M. Heimsath, and W. E. Dietrich (2005), Erosion of upland hillslope soil organic carbon: Coupling field measurements with a sediment transport model, *Global Biogeochem. Cycles*, *19*, GB3003, doi:10.1029/2004GB002271.

1. Introduction

[2] Recently, *Stallard* [1998] suggested that sediment disequilibria and crop replacement of eroded C in agricultural watersheds could globally sequester atmospheric CO_2 at the rates of 1–2 Gt C yr^{-1}, rates comparable to the size of so-called "missing C sink." Subsequently, a growing body of studies [*Harden et al.*, 1999; *Jacinthe et al.*, 2001; *Liu et al.*, 2003; *Manies et al.*, 2001; *McCarty and Ritchie*, 2002; *Ritchie and McCarty*, 2003; *Smith et al.*, 2001; *Starr et al.*, 2000] have followed *Stallard*'s [1998] work and have demonstrated the significance of agricultural soil organic carbon (SOC) erosion in the C cycle at numerous scales.

[3] Sediment transport, however, is also active on the steeply sloping landscapes of the world that are not suitable for cultivated agriculture. Most of the Earth's surface is not level, and landscapes with slopes less than 8% comprise only 36% of the global soils [*Staub and Rosenzweig*, 1992]. In sloping terrains, the impact of soil erosion on soil biogeochemistry has long been of interest [e.g., *Schimel et al.*, 1985, *Vitousek et al.*, 2003], although a process-based integration of sediment transport with soil biogeochemistry has not been attempted until recently. *Rosenbloom et al.* [2001] used a hillslope sediment transport model to understand the topographic distribution of soil texture and soil organic matter; the role of SOC erosion on undisturbed landscapes in a regional C budget has been recently studied [e.g., *Page et al.*, 2004; *Óskarsson et al.*, 2004]. However, it remains for researchers to quantify and integrate the rates of soil C erosion, deposition, and accumulation, and thus to determine the temporal dynamics of soil C storage within watersheds.

[4] Here we link sediment transport to the SOC cycle and extend *Stallard*'s [1998] hypothesis of an erosion-driven, nonsteady state SOC cycle to natural upland hillslopes that

0886-6236/05/2004GB002271$12.00

include both erosional and depositional landscape components. A comparative study was designed on two grass-covered hillslopes where recent research has empirically constrained a sediment transport model that could be combined with the soil C cycle. This work has three objectives: (1) to quantify the C erosion and deposition rates on different components of the landscape, (2) to integrate the landscape components to determine the net watershed C balance, and (3) to discuss the global implications of erosion-driven processes on watershed SOC storage. While this paper focuses on the temporal aspect of watershed SOC storage, our related paper [*Yoo et al.*, 2005] studies how sediment transport affects the spatial distribution of SOC storage in the same watersheds.

2. Conceptual Framework

2.1. Core Concept

[5] Soil mantled hillslopes are commonly coupled areas of erosional and depositional surfaces. Erosion and deposition carry SOC and, together with bedrock conversion to soil, determine soil thickness. A mass balance model of SOC must therefore include (1) inputs: depth-dependent plant C inputs and depositional SOC inputs; (2) losses: depth dependent microbial decomposition and erosional loss of SOC; and (3) soil thickness as a boundary condition for the soil C profile. This model can be expressed as

$$\frac{dS}{dt} = I - R - \varepsilon = \int_0^H \frac{I_z}{\Delta z} dz - \int_0^H k_z \rho_z C_z dz - \rho_E C_E E, \quad (1)$$

$$\frac{dH}{dt} = P - E, \quad (2)$$

and S is SOC storage [ML^{-2}], t is time [T], I is plant C input [$ML^{-2}T^{-1}$], R is heterotrophic respiration of C [$ML^{-2}T^{-1}$], ε is C erosion loss (positive) or depositional input (negative) [$ML^{-2}T^{-1}$], H is soil thickness [L], z is soil depth [L], Δz is the modeled soil depth layer [L], ρ is soil bulk density [ML^{-3}], k is the microbial decomposition rate [T^{-1}], C is the mass fraction of carbon in soil [MM^{-1}], E is soil erosion (positive) or deposition (negative) rate [LT^{-1}], P is bedrock to soil conversion rate [LT^{-1}], and the subscript E represents erosion or deposition. This SOC storage model uniquely includes not only the SOC erosion rate (ε), but also the soil thickness (H) defined as the balance of soil erosion and production.

[6] Along with the watershed SOC storage, we are interested in the net C flux from the atmosphere to soils as a function of landscape position. According to equation (1), the excess of plant C inputs over decompositional C losses (F_C: C sink when positive or C source when negative) can be described as

$$F_C = I - R = \frac{dS}{dt} + \rho_E C_E E. \quad (3)$$

This equation determines the size of the SOC sink (or source) for a landscape component (e.g., eroding slope) based on the rates of SOC storage change and C erosion (or deposition).

2.2. Soil Organic Carbon Erosion Model

[7] The models described above were applied to vegetated soil-mantled convex hillslopes where soil transport is caused by biological activity (e.g., animal burrowing, root decay, tree throw) or abiotic processes (e.g., rain splash or swelling/shrinking of clay-rich soils) [*Dietrich et al.*, 1995; *Roering et al.*, 2002]. Sediment flux in these situations depends on the slope gradient ($-\nabla Z$) [*Culling*, 1963],

$$\tilde{q}_s = K(-\nabla Z), \quad (4)$$

where $\tilde{q}_s$ is the volume of sediment crossing a unit contour line per unit time [L^2T^{-1}], K is the diffusivity [L^2T^{-1}], and $-\nabla Z$ is the slope gradient [unitless]. The soil erosion rate (E) at any location is the difference between inputs and outputs of sediment flux ($\tilde{q}_s$), and is thus curvature dependent,

$$E = \nabla \cdot \tilde{q}_s = K(-\nabla^2 Z), \quad (5)$$

where $-\nabla^2 z$ is the negative curvature of the ground surface (convex when positive, concave when negative) [L^{-1}].

[8] The amount of C carried with eroded soil is sensitive to the C content of the eroding soil (C_E in equation (1)). Since SOC concentrations vary significantly with depth, we need to know what soil depths contribute to soil erosion. In contrast to water runoff that removes the materials on the soil surface, diffusion-like sediment transport has a characteristic velocity depth profile that depends on the erosional agent [*Roering et al.*, 2002]. C_E can be estimated by equating the SOC transport ($\rho_E C_E \tilde{q}_s$) to a depth integrated SOC velocity profile,

$$\rho_E C_E K(-\nabla Z) = \int_0^H \rho_z C_z V_z dz, \quad (6)$$

where V is the sediment transport velocity [LT^{-1}]. When the depth profiles of soil bulk density, C concentration, and velocity are determined for a hillslope with known diffusivity, this relationship provides an estimate of C_E.

2.3. Soil Organic Carbon Storage in Accumulating Soil

[9] Vertical soil thickness (H) is calculated as the balance of soil erosion and production (equation (2)) [e.g., *Dietrich et al.*, 1995; *Heimsath et al.*, 1997]. Soil is defined as the disrupted material from bedrock that is susceptible to mass movement. The soil production rate decreases exponentially with soil thickness [*Heimsath et al.*, 2000, 2002, 1997, 1999, 2001]. If erosion rates are curvature-dependent, soil thickness is described as (Figure 1a)

$$\frac{\partial H}{\partial t} = \frac{\rho_r}{\rho_s} \varphi_0 e^{-H/\alpha} - K(-\nabla^2 Z), \quad (7)$$

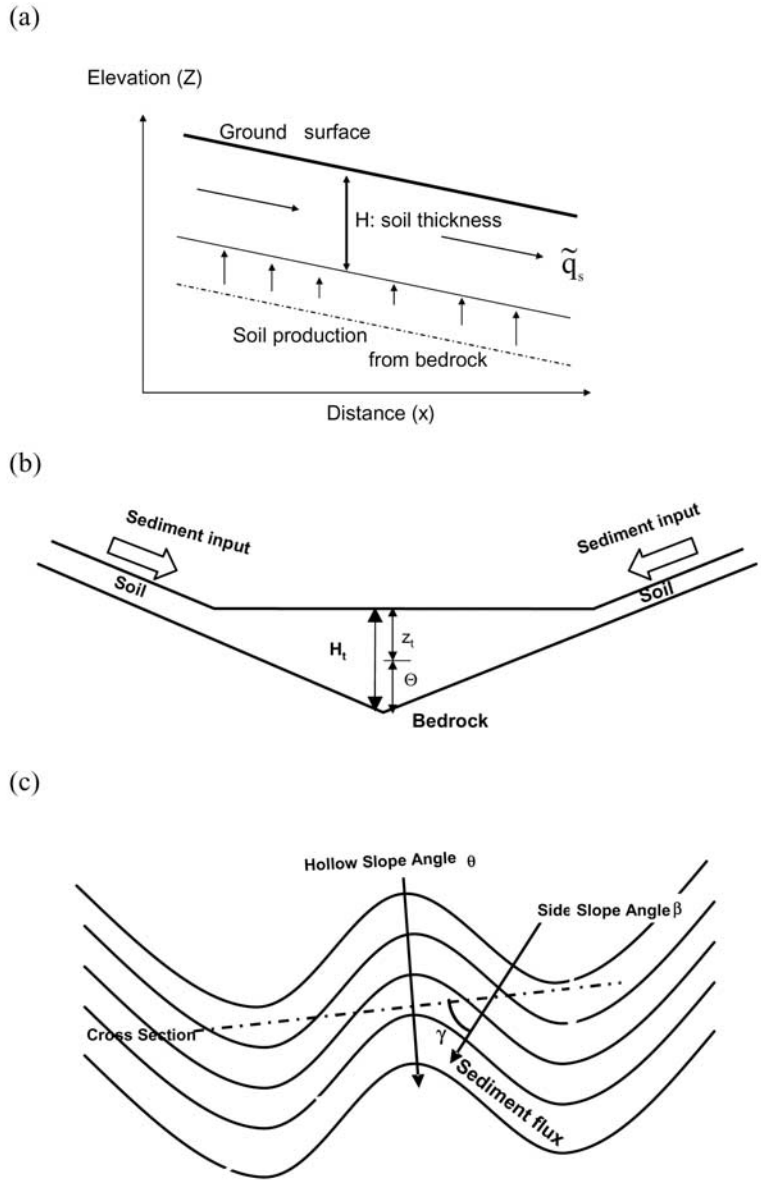

Figure 1. (a) A schematic diagram of the mass balance of hillslope soils affected by soil production and sediment transport, where $\tilde{q}_S$ is $K(-\nabla z)$ in equation (4) (modified from *Heimsath et al.* [1997]), (b) a cross-section view of the hollow, and (c) a plan view of the hollow from above. H is vertical soil thickness, z is depth from ground surface to soil layer of interest, Θ is the distance from the soil layer of interest to bedrock, β is side slope angle, and θ is hollow slope angle.

where φ_o is the soil production rate for exposed bedrock [LT^{-1}], α is the e-folding depth of the soil production rate [L], and the subscripts *r* and *s* represent bedrock and soil, respectively.

[10] While a steady state soil thickness may develop on convex hillslopes, soils on concave surfaces ($-\nabla^2 z$ is negative) thicken owing to continuous sediment input. In hollows, the soil thickening rate hinges on hillslope geometry (Figures 1b and 1c) and diffusivity. On the basis of work by *Dietrich et al.* [1986], the vertical soil thickness along a hollow axis is a function of diffusivity (*K*), side slope angle (β), hollow slope angle (θ), and time (*t*),

$$H_t = \sqrt{2Kt}\left[\left(\tan^2\beta - \tan^2\theta\right)\left(\frac{1}{\cos^2\beta} - \frac{1}{\cos^2\theta}\right)\right]^{1/4}. \quad (8)$$

[11] To simulate the SOC storage during sedimentation (equation (1)), we also need to model the plant C input and decomposition rates and parameterize them with field and laboratory measurements. The plant C input (I_z) [g C m^{-2} yr^{-1}]

between soil depths of z and $z + \Delta z$ [cm], and the decomposition rate (k_Z) [yr^{-1}] at depth z are described as exponentially decreasing with soil depth,

$$I_z = I_o \exp\left[-\left(z + \frac{\Delta z}{2}\right)/\eta\right] \quad (9)$$

$$k_z = k_o \exp[-z/\kappa], \quad (10)$$

where subscripts o represent their surface values, and η and κ represent e-folding depths of root C input and decomposition rates, respectively.

[12] The depth z of root C inputs and decomposition rates is adjusted as soil thickens in modeling SOC storage (equation (1)). Since the distance of a certain soil layer to bedrock (Θ) remains constant despite the soil thickening (e.g., soil production rate is nearly zero under thick depositional soils since the soil production rate decreases exponentially with increasing soil thickness [*Heimsath et al.*, 1997]) (Figure 1b), the depth z is described as

$$z = H_t - \Theta. \quad (11)$$

3. Methods

3.1. Study Area

[13] We studied two watersheds in central California. The primary study site is Tennessee Valley (TV), Marin County. The area is underlain by Jurassic-Cretaceous Franciscan greywacke sandstone, and the climate is Mediterranean with a mean annual precipitation (MAP) of 1200 mm and a mean annual temperature (MAT) of 14°C (nearby Kensfield weather station). Vegetation is a mixture of annual and perennial grasses with varying densities of coastal shrub. Grazing was practiced through the nineteenth and early twentieth centuries, but was eliminated in 1972 [*Dietrich et al.*, 1995]. At TV, soil production and transport are primarily driven by pocket gopher burrowing: Gophers physically disrupt saprolite [*Heimsath et al.*, 1997], and this soil perturbation, aided by gravity, results in net downslope sediment transport [*Black and Montgomery*, 1991]. In contrast, runoff experiments at TV showed that soil erosion by overland flow is negligible [*Prosser and Dietrich*, 1995; *Prosser et al.*, 1995]. The average slope on the studied zero-order watershed is 30%. The intense soil mixing by gophers [*Black and Montgomery*, 1991] produced weakly developed soils with thick, dark A horizons overlying a weathered bedrock. We classified the soils as Lithic Haplustolls to Lithic Ustorthents on convex slopes and Oxyaquic Haplustolls in hollows.

[14] The complementary site is Black Diamond Regional Preserve (BD), Contra Costa County located approximately 80 km east of TV. In contrast to TV, soft Eocene clay-rich marine shale composes the bedrock. The climate is also Mediterranean, but is drier and warmer than TV (MAP = 330 mm, MAT = 16°C) (nearby Antioch Pump Plant weather station). Annual grasses are dominant, and grazing is currently limited to winter months. The abiotic processes of clay hydration and dehydration cause clay-rich bedrock to break down to soil, and the shrinking and swelling of the clay-rich soils causes soil creep [*McKean et al.*, 1993]. While biotic soil perturbation occurs, the abiotic soil creep dominates erosive transport. Soil erosion by overland flow is negligible [*McKean et al.*, 1993]. The average slope of the area is 25%. The vertical soil mixing by shrinking and swelling results in thick A horizons overlying soft bedrock. We classified the soils as Typic Haploxerolls on summit hillslopes to Typic Haploxererts on shoulders to footslopes.

3.2. Field and Laboratory Measurements

[15] A topographic survey with a total laser station (Sokkia Co., Ltd.) at a 1–2 m interval was made to obtain coordinates of the ground surface for calculating slope gradient and curvature. The survey resulted in ~4000 survey points within ~8000 m^2 of the zero-order watershed at TV and ~1700 points within ~3500 m^2 of the hillslope transect at BD. The survey points were gridded using a Krigging method to generate topographic maps. In calculating curvature, we followed a method described by *Heimsath et al.* [1999] using Surfer® software.

[16] Soils and bulk density cores were sampled to the bedrock-soil interface in both convex and concave areas (Figures 2a and 2b). At BD, channels invaded into all of the surveyed hollows, indicating the importance of overland flow. Thus we avoided hollows and focused on the areas dominated by diffusive sediment transport. Soil pits were excavated along a hillslope transect from summit to footslope (Figure 2b) [*Ruhe and Walker*, 1968]. To facilitate the spatial analyses, soils were sampled at predetermined depth intervals rather than by horizons. The thicknesses of the depth increments increased from 5 cm at the soil surface to 20 cm after 50 cm. In the TV hollow, where greater horizonation was present, sampling was by soil horizon to capture more pedological information.

[17] A representative ~200 g of soil was obtained from air-dried bulk soil samples using a soil splitter, and was then passed through a 2-mm sieve. An ~40 g of the <2-mm fraction was used for particle size analysis, and 10-g subsamples were used for C and N analysis. The 10-g subsample was ground with corundum pellets on a roller mill prior to C and N analysis. At BD, we removed the inorganic carbon in the calcareous soils using HCl fumigation [*Harris et al.*, 2001].

[18] Three quadrat (0.25 m × 0.25 m) of standing biomass were harvested within 3 m of all soil pits excavated for C analysis (Figures 2a and 2b) at the end of the growing season (late May) for 3 years (2001–2003). Plant samples were oven-dried (60°C) for 24 hours and then weighed. Partially decomposed biomass from the previous year was removed prior to weighing. Plant samples for C and N analyses were ground using a Wiley mill, and were then ground in 5-g aliquots using a SPEX 6800 cryogenic grinding mill until all fibrous materials had disappeared.

[19] The C and N content of soil and plant samples were measured using a Carlo Erba CN analyzer. Atropine was

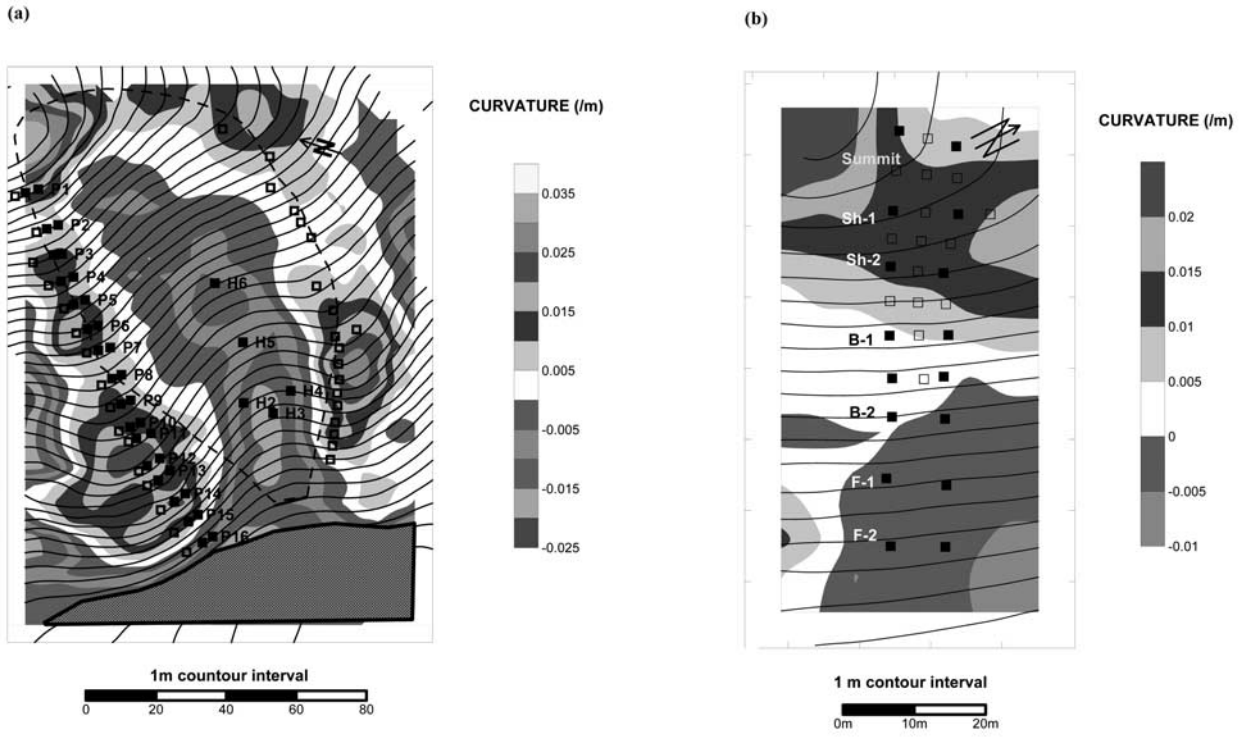

Figure 2. Map of study sites. (a) Tennessee Valley and (b) Black Diamond. The solid squares represent soil pits where samples were taken. The open squares represent sites where only soil thicknesses were measured. The dashed line at TV defines the boundary of the zero-order watershed. See color version of this figure at back of this issue.

used as a standard. Particle size was determined by the hydrometer method [*Day*, 1965] following pretreatments with H_2O_2 for organic matter removal and $(NaPO_3)_6$ for clay dispersion. Soil cores for bulk density determination (5 cm id × 5 to 15 cm length depending on the thickness of measured soil layer) or peds (a structural unit) were oven dried at 110°C for 24 hours and then weighed for bulk density. In the case of peds, volume was determined by displacement in water. Bulk density samples were corrected for rock fragments (>2 mm).

4. Model Parameterization

4.1. C Erosion Model

[20] The values used to parameterize the C erosion model (equation (5)) are given in Table 1. The C content of

Table 1. Parameters for Calculating the Soil C Erosion Fluxes at Tennessee Valley and Black Diamond and the Accumulation of Hollow SOC at Tennessee Valley

Parameter	Tennessee Valley	Black Diamond
K (equation (4))	50 $cm^2\ yr^{-1}$ [a]	360 $cm^2\ yr^{-1}$ [b]
φ_o (equation (7))	77 ± 9 m Myr^{-1} [a]	~1255 m Myr^{-1} [b]
α (equation (7))	0.23 ± 0.003 m[a]	~0.27 m[b]
C concentration of eroding soils (C_E in equation (1))	case I: $C_{5-15} = 0.01 \times (2.0060 + 0.0202Z)$, case II: $C_{0-5} = 0.01 \times (3.5615 - 0.0526Z + 0.0035Z^2)$, Z: elevation (m)	decreasing from 2% at summit to 0.7% at footslope
Bulk density of eroding soil	1.25 g cm^{-3}	1.36 g cm^{-3}
Hollow soil thickness and C accumulation	side slope (β): 18° (H3) 17° (H5), convergence angle (α): 52° (H3) 72° (H5), $I_z = 179e^{-z/10}$ g C $m^{-2}\ yr^{-1}$, $k = 0.09e^{-z/13}\ yr^{-1}$	N/A

[a] *Heimsath et al.* [1997].
[b] *McKean et al.* [1993] (P_o and α are calculated from *McKean et al.* [1993]).

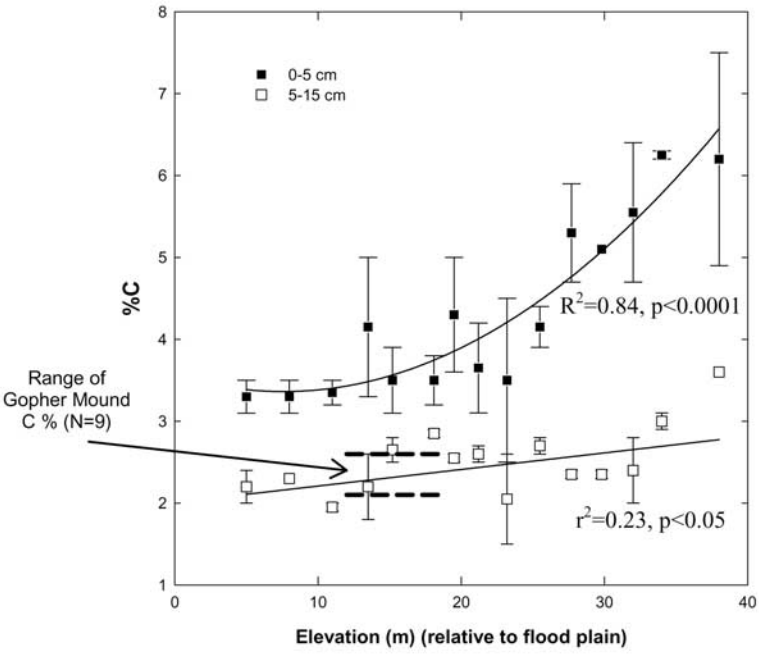

Figure 3. Carbon contents of the top two soil layers regressed against elevation at Tennessee Valley. The relationships between C% and elevation are in Table 1.

sediment at TV was bracketed using two end-member values. Case I assumes that soil transport occurs throughout the soil profile by gopher burrowing and mounding [*Black and Montgomery*, 1991; *Heimsath et al.*, 1997]. We used the C% of the 5–15 cm soil depth, where gophers concentrate their burrowing activity [*Reichman and Seabloom*, 2002], which was found to be close to the C% of fresh mounds (Figure 3). Additionally, we note that if the sediment transport velocity decreases linearly with soil depth (equation (6)), the resulting depth-weighted C% is similar to the C% of the 5–15 cm soil depth. Case II reflects the transport of the soil surface, and uses the C% of the 0–5 cm soil depth. Given the known dominance of gopher burrowing in soil transport, case II serves as a high end estimate. The measured C% of the 0–5 cm and the 5–15 cm systematically varied with elevation (Figure 3), while no significant correlation existed with slope or curvature. The fitted relationships between C% and elevation were used in determining the C% of eroding soils over the entire zero-order watershed. For areas above and below the elevations covered by the relationship, the nearest measured soil C% was used.

[21] At BD, as reported by *McKean et al.* [1993], soil transport velocity is assumed to linearly decrease from a maximum at the soil surface to zero at the soil-bedrock interface (equation (6)). This corresponds with field observations that soil cracking decreases with depth. Using known diffusivities and measured bulk densities and slope gradients (Table 1), the calculated sediment C% decreases from 2% at the summit to 0.7% on the footslope owing to the following reasons. First, the measured ANPP decreased in a downslope direction. Second, as soil thickens in the downslope direction, the contribution of deeper soil layers, with low C%, to sediment transport increased (equation (6)).

4.2. Soil C Accumulation Model at Tennessee Valley

[22] The TV hollow SOC storage was simulated at 5-cm-depth intervals for every 5 years after parameterizing the model components (equations (1) and (8)–(11)). The parameters are listed in Table 1. We assumed that the hollow was entirely evacuated at some time = 0, based on the observed absence of a buried A horizon or an irregular vertical pattern of C content and soil texture. Additionally, all the hollow soils had similar weakly developed profiles suggesting relative youthfulness. The soil thickness during the hollow infilling was simulated for two locations: H3 and H6, both along the hollow axis (Figure 2a). From the map survey, we determined the slope angles used in equation (8).

[23] The exponential function of root C inputs and its e-folding depth (equation (9)) were determined based on the observation that root densities decrease rapidly with soil depth between 5 and 15 cm. For I_o, we used the averaged value of measured hollow ANPP (179 g C m^{-2}). With these parameters, the 1-m-depth integrated belowground root C input is approximately twice the size of measured ANPP, which is slightly higher than values (1.1–1.7) reported for one annual grassland in central California [*Baisden et al.*, 2002a] but is lower than the global estimate for temperate grasslands (3.7) [*Jackson et al.*, 1996].

[24] The exponential decomposition rate model (equation (10)) is reasonable since deep soil horizons in hollows have seasonal anoxic conditions due to subsurface waterflow (reflected by gray colors). To determine k_o, we

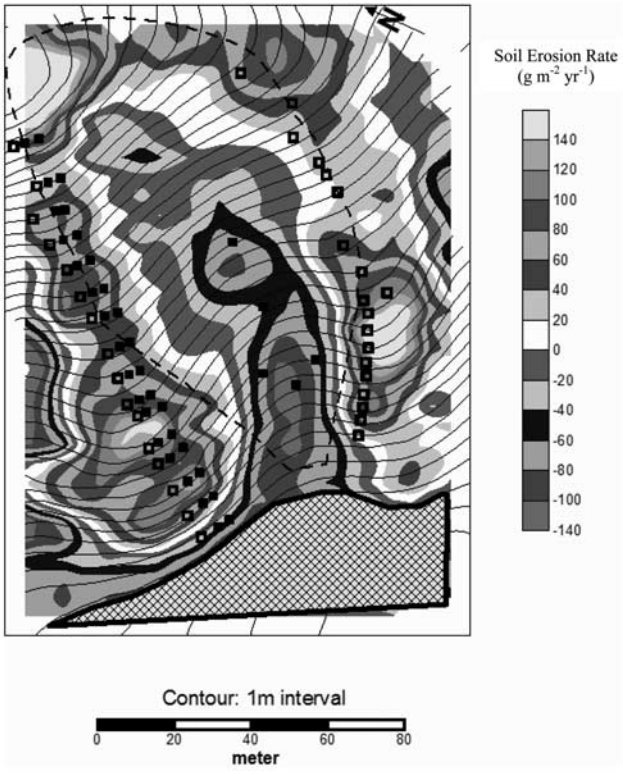

Figure 4. Calculated soil erosion rates at Tennessee Valley. A negative quantity indicates deposition. The floodplain (hatched area) is not included in the calculation. See color version of this figure at back of this issue.

used a steady state first-order decay model such that $dC/dt = I - k_o C = 0$, where C is the C content of soil surface (0–5 cm, 2.0 kg C m^{-2}) and I_o is the measured ANPP. The e-folding depth was chosen to fit the measured C profile. We will later address the ramifications of the single versus multiple pool C approaches [e.g., *Trumbore*, 1993; *Trumbore et al.*, 1996, 1989]. Bulk densities were measured to be 1.3 ± 0.05 g cm^{-3} (n = 16) and 1.7 ± 0.04 g cm^{-3} (n = 12) for the upper 50 cm and greater depths, respectively, and the soil thickening rate was adjusted to bulk density changes during the sedimentation.

5. Results and Discussion

5.1. Erosion and Deposition Processes

5.1.1. Soil Erosion and Deposition

[25] At TV, the calculated soil erosion rates are as high as 140 g m^{-2} yr^{-1} on the most convex portions of the hillslope, while the deposition rate achieves values as high as 140 g m^{-2} yr^{-1} in the hollow axis (Figure 4). Within the boundaries of this zero-order watershed (Figure 2a), we integrated the soil erosion for the convex slopes and obtained a value of ~200 kg yr^{-1}. To quantify the sediment exported from the watershed, we calculated the sediment transport crossing the lower boundary of the hollow (Figure 2a) by using equation (4) (with a bulk density of 1.25 g cm^{-3} and diffusivity of 50 cm^2 yr^{-1}), and obtained a rate of 12.5 kg yr^{-1}, suggesting that most (~94%) of the eroded soils are redistributed within the watershed. In these calculations, we assumed that the rate of topographic change on the convex slope is not large enough to significantly affect our calculations of soil erosion rates for timescales of 10^4 years, time periods that encompass hollow accumulation and evacuation. This is partly supported by investigations of the timescales needed to achieve steady state soil thickness (~10^3 years) [*Dietrich et al.*, 1995] versus steady state hillslope morphology (10^6 years) [*Fernandes and Dietrich*, 1997] at TV.

[26] At BD, the soil erosion losses are reported along a two-dimensional hillslope transect because there was minimal horizontal convexity (Figure 5a). The calculated erosion rate for the shoulder is nearly 700 g m^{-2} yr^{-1}, while the footslope accumulates sediment at rates of up to 200 g m^{-2} yr^{-1} (Figure 5b), which is considerably greater than at TV. By integrating the soil erosion rates on the upper convex area, we obtained rates of ~27 kg m^{-1} yr^{-1} as the sediment input to the depositional slope. This sediment input can be also estimated with slope-dependent sediment transport (equation (4)). By multiplying the slope gradient between B1 and B2 (transition between convex to convergent slope) using a bulk density of 1.36 g cm^{-3} and diffusivity of 360 cm^2 yr^{-1}, the rate is ~16 kg m^{-1} yr^{-1}. This difference may reflect an ongoing morphological change of the hillslope. Given the uncertainties in hillslope evolution, we consider 16–27 kg m^{-2} yr^{-1} as the range of sediment inputs to depositional areas at BD. Of this annual sediment flux, about 5 kg (19–33% of eroded sediment) accumulates within the footslope (Figure 5a), while the remainder reaches the toeslope below the study area in Figure 2b.

[27] These two hillslopes represent a wide spectrum of natural hillslope erosion rates [*Heimsath et al.*, 1999]. However, even the highest erosion rates on the most convex portions are lower than the agriculture-induced erosion rates averaged across the conterminous United States (~940 g m^{-2} yr^{-1}) [*Smith et al.*, 2001]. Additionally, most of the eroded sediment is redeposited within the zero-order watersheds and does not reach the streams. Below, we quantify the amount of C moving with eroded soils.

5.1.2. C Erosion Loss and Depositional Input

[28] At TV, the SOC erosional loss was estimated to be up to 6 g C m^{-2} yr^{-1} (case I) or 16 g C m^{-2} yr^{-1} (case II) on the most convex slopes (Figures 6a and 6b). In the hollows, the depositional C input was as high as 3.0 g C m^{-2} yr^{-1} (case I) or 6.0 g C m^{-2} yr^{-1} (case II) near the hollow axis (Figures 6a and 6b). At BD, with higher soil erosion rates and lower soil C%, the SOC erosional loss is up to 13 g C m^{-2} yr^{-1}, while the depositional C input ranged between 0 and 2 g C m^{-2} yr^{-1} on the footslope (Figure 5b).

[29] The C erosion losses were integrated over the entire area of convex slopes, and this value was divided by the area of the slopes to obtain the average C erosion loss. At BD, as was done for the soil erosion calculations above, we also used a slope dependent sediment transport model (equation (4)) to calculate the C erosion input from B1 to B2. The resulting averaged C erosion losses from convex slopes are between 1.4 and 2.7 g C m^{-2} yr^{-1} at TV and 5

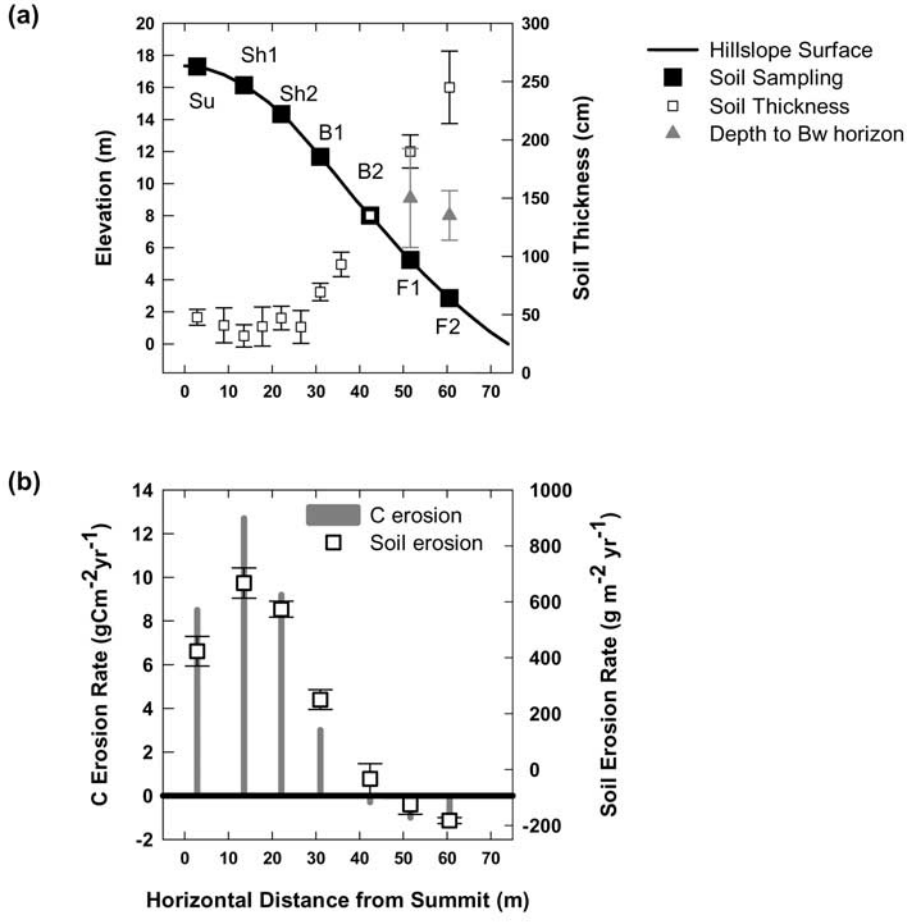

Figure 5. Black Diamond hillslope transect. (a) Sampling locations, soil thickness, and depth to Bw horizons. (b) SOC and soil erosion losses. The error bars are calculated from replicate soil pits at the same elevation (Figure 2b). Negative quantities indicate deposition.

and 8 g C m^{-2} yr^{-1} at BD. At TV, we calculated the C export from the zero-order watershed by multiplying the sediment transport through the lower boundary of the hollow by the C% of sediment (2.3% for case I and 5% for case II) and then dividing it by the watershed area. The resulting C export is 0.04–0.08 g C m^{-2} yr^{-1}.

[30] While the comparison of calculated C erosion rates with previous studies is in order, it is important to state that the C loss via diffusive soil erosion has not been attempted before. Thus this is the first comparison between very different approaches to quantifying SOC losses from uplands. *Stallard* [1998] estimated C export of 1–5 g C m^{-2} yr^{-1} from undisturbed watersheds on a global basis. These estimates were based on stream sediment yield, and thus they conceal the spatial redistribution of eroded sediment not only within the watershed, but within hillslopes above the channels. Our values (see previous paragraph) are several orders of magnitude lower. However, we will show later that the long-term (a period considering the cycle of hollow evacuation and infilling) averaged C export from the TV watershed is ~0.8 g C m^{-2} yr^{-1}, a value close to the low end of *Stallard*'s [1998] estimate.

[31] Our study illustrates the importance of the sediment transport mechanism in determining C erosion losses. Black Diamond, despite a lower C%, had a higher erosive C loss due to much higher diffusivity (Table 1). The role of the sediment transport mechanism would be even more pronounced if we compared diffusive to runoff driven transport. Runoff preferentially removes finer soil particles from the ground surface, which tend to be enriched in C [*Liu et al.*, 2003; *Walling*, 1983]. In contrast, diffusive sediment transport tends to be less efficient in particle size sorting, and its effect varies with depth depending on the responsible agent [*Roering et al.*, 2002]. Additionally, curvature-dependent soil erosion is independent of hillslope scale, while the eroding power of overland flow increases with drainage area.

5.1.3. C Erosion and Deposition Versus Measured Plant C Input

[32] The relative importance of the C erosion losses in the soil C cycle were made by comparing them to the measured ANPP during 2001 and 2002. At TV, on the most convex portions of the hillslope, erosional losses of C were up to 5% (case I) and 14% (case II) of the ANPP. While the

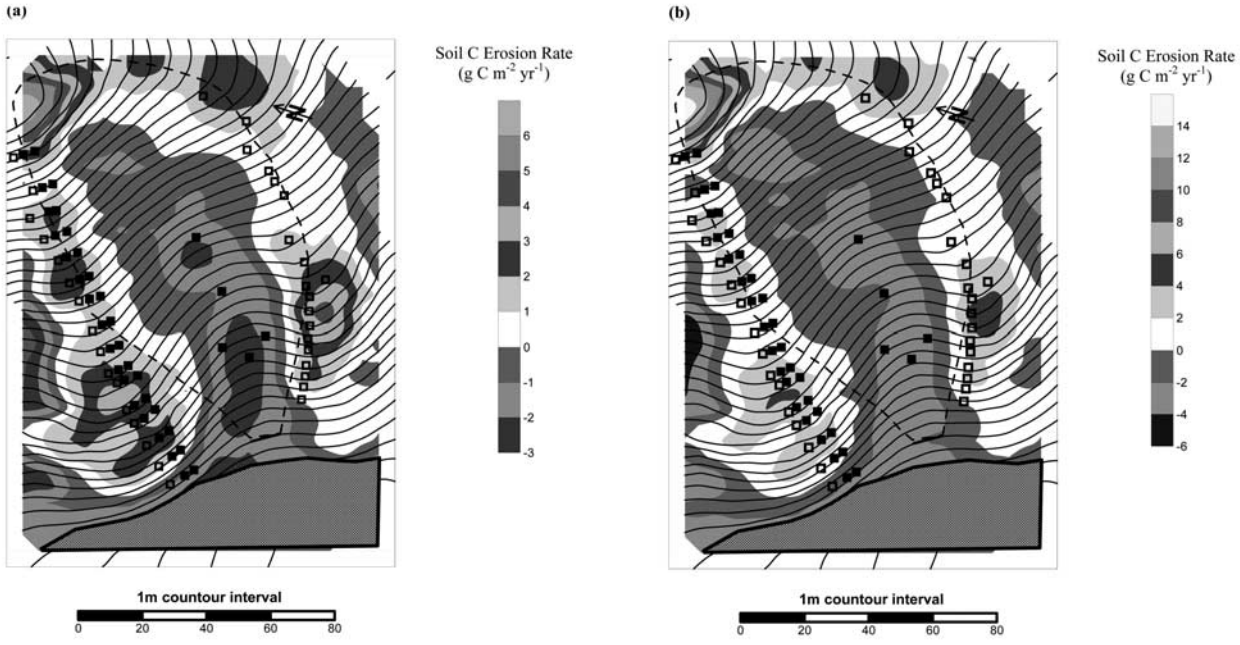

Figure 6. SOC erosion loss at Tennessee Valley. (a) Case I. (b) Case II. Negative quantities indicate deposition. The floodplain (hatched area) is not included in the calculation. See color version of this figure at back of this issue.

erosional loss of SOC increases with convexity (Figure 7a), ANPP tends to decrease slightly (Figures 7b and 7c), thereby increasing the impact of erosion on the local SOC budget with increasing slope convexity. In the adjacent hollow, the depositional C input ranges between 1 and 2% of measured ANPP. As background, we note that the ANPP measurements at TV included years with greatly varying precipitation. Since ANPP in 2001–2002 was significantly lower than that of the wetter 2003 growing seasons (Figure 7c), the calculated fractions of SOC erosion to ANPP are upper end estimates.

[33] At BD, ANPP is reported for 2003, the year that grazing did not occur. On the basis of these data, soil erosion appears to remove C at a rate of up to 7% of the ANPP on the most convex slope positions (Figures 7d and 7e). In contrast, the depositional C inputs are ~1% of the in situ ANPP. Given that the year 2003 was relatively wet and thus produced high biomass, these relative percentages are likely to be minimum values.

5.2. Temporal Trend of Soc Storage

5.2.1. Steady State Soil Organic Carbon Storage on Convex Slopes

[34] In spite of continued C erosion losses, the convex slopes have likely maintained steady state SOC storage over a $\sim 10^3 - 10^4$ year scale (the timescale that depositional slopes accumulate SOC, discussed in the following section). Since SOC storage is determined by soil thickness and the C profile, below we examine the possible temporal changes of these two factors.

[35] First, we examined whether the measured soil thickness conforms to predicted steady state relations where soil thickness varies with curvature (i.e., where equation (7) = 0). At TV, the soil thickness, though containing significant scatter, is indeed correlated with curvature (Figure 8a). The scatter is likely due to the highly stochastic nature of gopher burrowing activity and the heterogeneity of Franciscan greywacke bedrock [*Heimsath et al.*, 1997]. At BD, the agreement between measurements and the modeled steady state soil thickness is quite good (Figure 8b), probably owing to a more spatially homogenous abiotic soil creep and soil production.

[36] Secondly, because the soil C concentrations (% C) do not respond to slope gradient and curvature at the studied sites [*Yoo et al.*, 2005], this suggests that biological C cycling, rather than sediment transport or soil erosion, determines soil C%. We know little about the temporal trends of biological C cycling in the past 10^3 to 10^4 years. Instead, given the likely steady state soil thicknesses on the convex slopes and the observed homogeneous sedimentation record in the excavated hollow and footslope soil pits, it appears that the climate variability has never been severe enough to disrupt soil transport during the sediment accumulation in depositional slope positions ($10^3 - 10^4$ years, discussed below). Given these observations, we suggest that SOC storage on convex slopes has been largely in steady state for the timescale of interest ($10^3 - 10^4$ years).

5.2.2. Soil Organic Carbon Accumulation in Depositional Slopes

[37] In contrast to convex slopes, convergent areas have thicker soils due to continuous deposition (Figures 8a and 8b). To estimate the SOC accumulation rates in hollows or depositional segments of the landscape, the age of the deposit must be determined. A simulation of the hollow soil

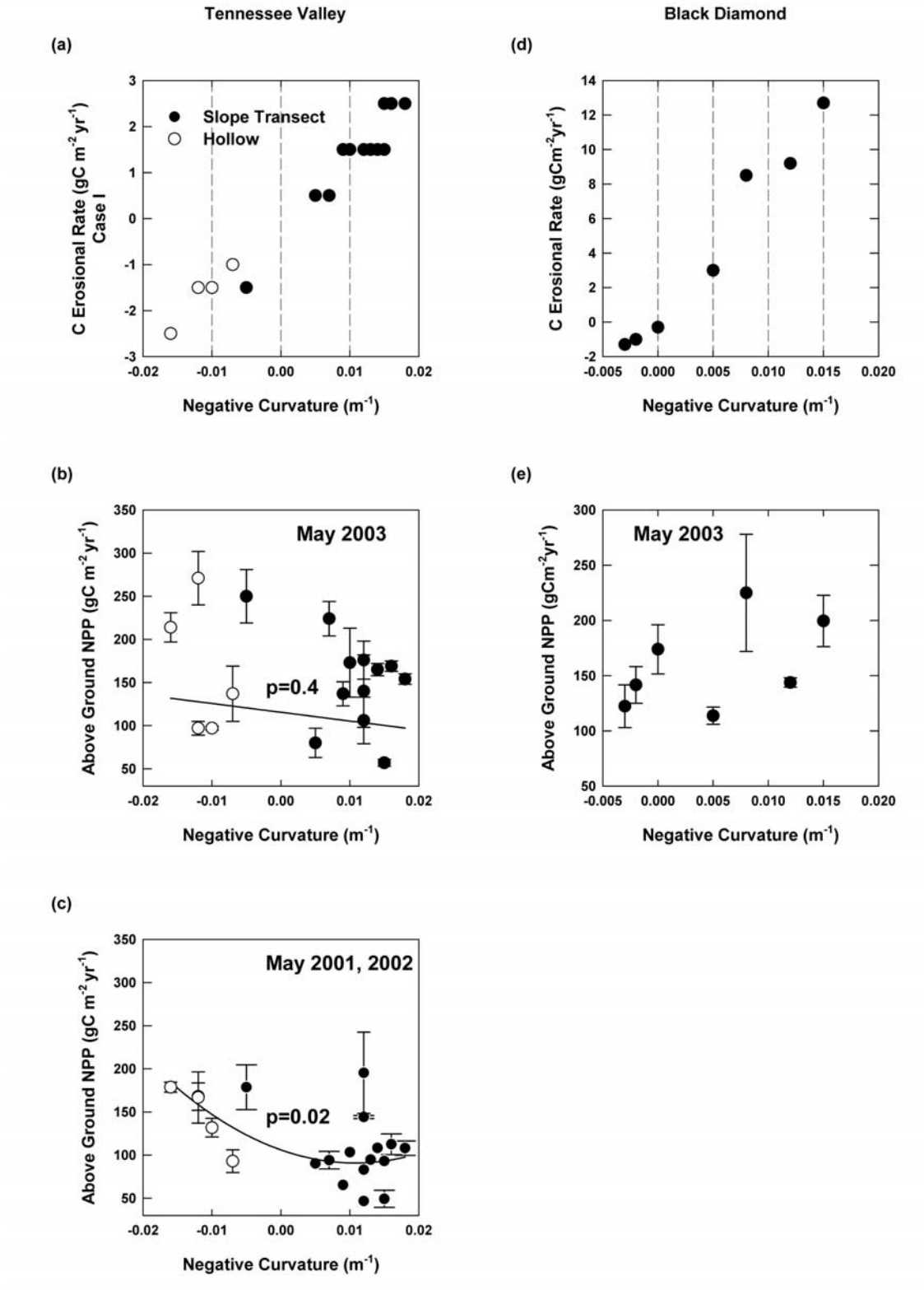

Figure 7. SOC erosion loss and above ground NPP versus curvature. (a, b, c) Tennessee Valley. (d, e) Black Diamond.

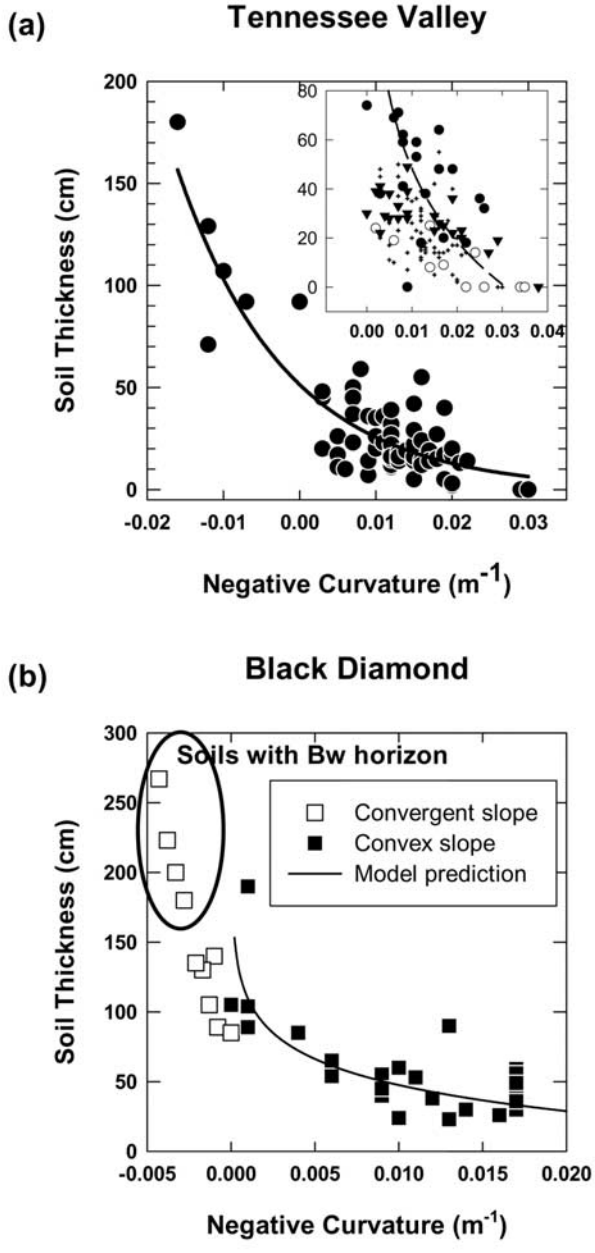

Figure 8. Soil thickness versus negative curvature. (a) Tennessee Valley. (b) Black Diamond. The inset of Figure 8a focuses on the soil thickness versus curvature relationship at convex slopes, where the different symbols represent individual hillslopes within Tennessee Valley. The line in the inset is the model prediction (equation (7)). Tennessee Valley data from *Heimsath et al.* [1997] are included in the inset as solid circles and triangles.

thickness at TV (equation (8)) suggests that 11–13 kyr would be required to fill the hollow to the current thickness (Figure 9a), consistent with the published hollow ages in the area determined by dating basal charcoal [*Reneau and Dietrich*, 1990; *Reneau et al.*, 1990, 1986]. Additionally, the soil thickening rate (the slope of soil thickness versus time in Figure 9a) rapidly decreases as sediment is distributed over an expanding hollow area.

[38] The age of the soils on the depositional footslope at BD was also estimated. At BD, only the near-surface 1.5 m thickness of the footslope soil appeared mobile, because all four footslope soil pits (Figures 5a and 8b) showed the transition from dark A horizons with active mixing to weakly weathered Bw horizons at this depth. The soil eroded from the upper convex hillslope was determined to be 16–27 kg m^{-1} yr^{-1}, as discussed earlier in this paper. This sediment influx would fill the mobile soil layer of the

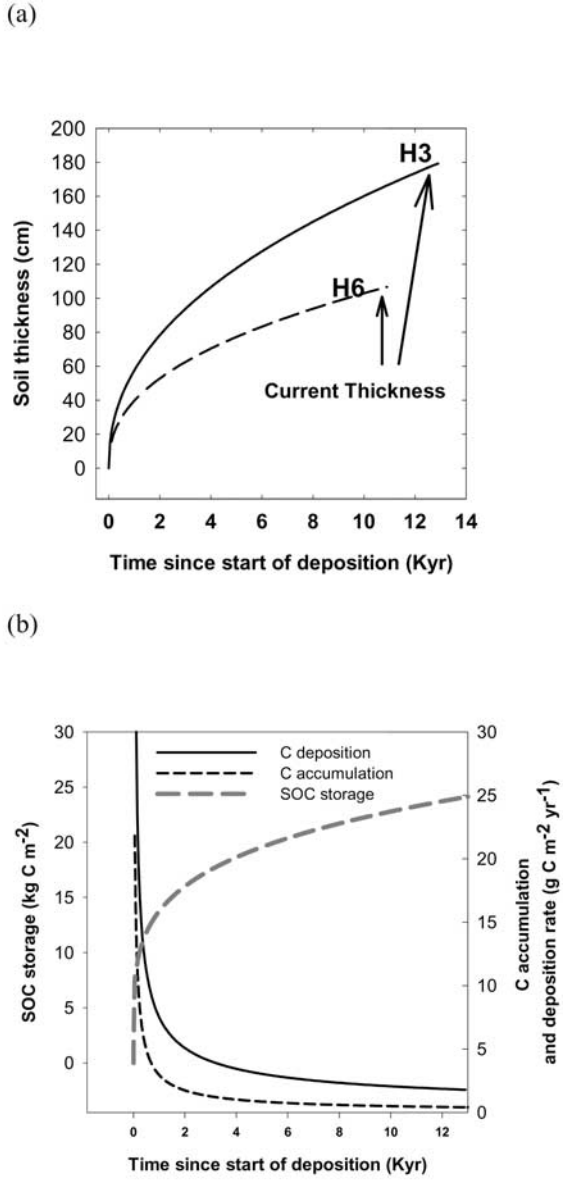

Figure 9. (a) Simulated hollow soil thicknesses at Tennessee Valley as a function of time since evacuation. H3 and H6 represent hollow soil pits (Figure 2a). (b) Simulated SOC storage, accumulation rates, and deposition rates during hollow infilling.

entire ~70 m length of the depositional slope (from site B2 to the channel) within 5.3–8.8 kyr, suggesting a mid-Holocene age for the depositional soils, a time consistent with likely Holocene changes to the adjacent floodplain level, which sets the hillslope boundary condition.

[39] The continuous accumulation of sediment leads to an ongoing accumulation of organic C in the depositional areas. The long-term C accumulation rate was calculated. At TV, the SOC storage of 5 excavated hollow pits ranged from 16.6 to 24.3 kg C m^{-2}. With a hollow age of about 12 kyr (Figure 9a), the long-term SOC accumulation rates vary between 1.4 and 2.1 g C m^{-2} yr^{-1}. In the BD footslope (F1 and F2 in Figure 5a), 15.0 ± 0.39 kg C m^{-2} (n = 4) is stored in the upper 150 cm of the soil. Dividing the SOC storage by the residence time (5.3–8.8 kyr), a long-term C accumulation rate of 1.7–2.8 g C m^{-2} yr^{-1} is obtained, which is similar to that in the TV hollow.

[40] Besides the long-term C accumulation rate, what has been the temporal trend of hollow C storage and accumulation rates? A model simulation for TV hollow SOC storage (equation (1) combined with soil thickness and biological C flux models from equations (8)–(11)) suggests that the SOC storage and accumulation rate has changed significantly during the course of hollow infilling (Figure 9b). A simulation at H3 shows a rapid initial accumulation (~60% of SOC storage occurs during the first 1000 years): C accumulation rate declines from the averaged rate of 14 g C m^{-2} yr^{-1} during the first 1000 years to 0.3 g C m^{-2} yr^{-1} at present (Figure 9b).

[41] The simulation of the C profile (without integration of equation (1)) (Figure 10) suggests that the soil surface C profile at TV hollow, once established, varies little with time as burial proceeds because C cycling rates (empirically parameterized plant C input and decomposition rate profiles) are faster than sediment deposition. As time progresses, the deeper soil zones with low C percentages thicken, resulting in the additional SOC storage. This process, combined with the declining rate of soil thickening, explains why SOC accumulation decreases faster than the soil thickening rate during hollow infilling (Figures 9a and 9b).

[42] Temporal carbon storage modeling was not undertaken for the BD footslope owing to the uncertainties in the initial condition of the footslope, but the current C accumulation rate is suggested. Presently, ~200 g m^{-2} of soil accumulates on the footslope annually (Figure 5b). As shown for the TV hollow, we assumed that fast biological C cycling at BD (suggested by its drier and warmer climate) primarily determines near-surface soil C, regardless of soil thickening rates, so that the extension of deep soil causes the SOC accumulation. The current C accumulation rate can be obtained by multiplying the soil deposition rate of 200 g m^{-2} yr^{-1} by the C% of the deepest layer in the footslope soils (0.39%). The result is a C accumulation rate of 0.8 g C m^{-2} yr^{-1}. This is smaller than the long term accumulation rate of 1.7–2.8 g C m^{-2} yr^{-1} estimated above, suggesting a decreasing C accumulation rate with time, as was suggested for the TV hollow.

[43] This work quantitatively illustrates that a dynamic, nonsteady state SOC storage occurs in depositional areas owing to sediment transport. We used our results from the two depositional slopes to provide some guidance in constraining the possible range of depositional SOC storage on a global scale. Of the uncultivated upland ecosystems (105.6×10^6 km^2 [*Post et al.*, 1982]), ~64% have slopes greater than 0–8% [*Staub and Rosenzweig*, 1992]. Assuming that 50% of these areas are depositional (53% at TV and 75% at BD) and have an average SOC storage of 10–20 kg C m^{-2} (the globally averaged SOC storage is 10 kg C m^{-2} from *Post et al.* [1982]), 340–680 Gt C may be stored in undisturbed upland depositional areas. Given the estimated residence time of the TV hollow (12 kyr) and BD footslope (5.3–8.8 kyr), 24–48% of 1400 Gt C [*Post et al.*, 1982] of the global SOC pool may reside in deposits that turnover at the timescales of 10^3 to 10^4 years.

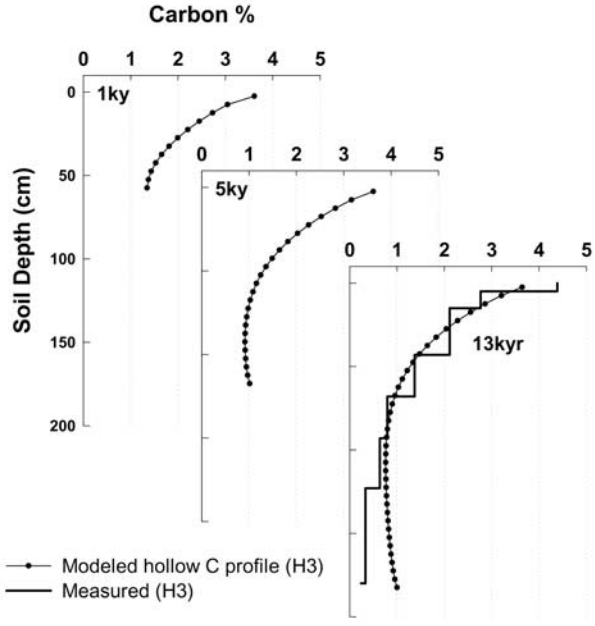

Figure 10. Simulated SOC profiles during the hollow infilling.

5.2.3. Watershed Soil Organic Carbon Storage

[44] Because zero-order watersheds have areas of both erosion and deposition, it is important to consider the SOC storage of the entire watershed over the timescales covering hollow infilling and evacuation (Figure 11a). For TV (the site most appropriate for this analysis), it was estimated earlier in this paper that the convergent hollow evacuated 12 kyr BP. The SOC stored in the hollow was estimated to be 73 t C based on the survey and soil C profile measurements. The SOC stored within the convex slope area was estimated to be 22 t C (obtained by multiplying the 6 kg C m^{-2}, an average of 31 convex slope soil pits, by 3734 m^2, the area of convex slope). The temporal trend of SOC accumulation in the hollow was based on the simulation made for site H3 (Figure 9b).

[45] The resulting diagram (Figure 11a) shows that the watershed SOC storage is largely driven by the hollow

(a)

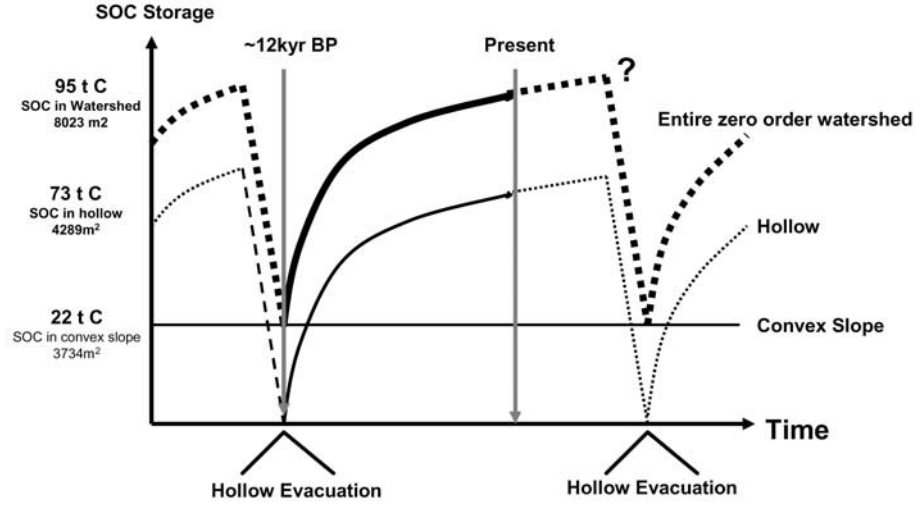

(b)

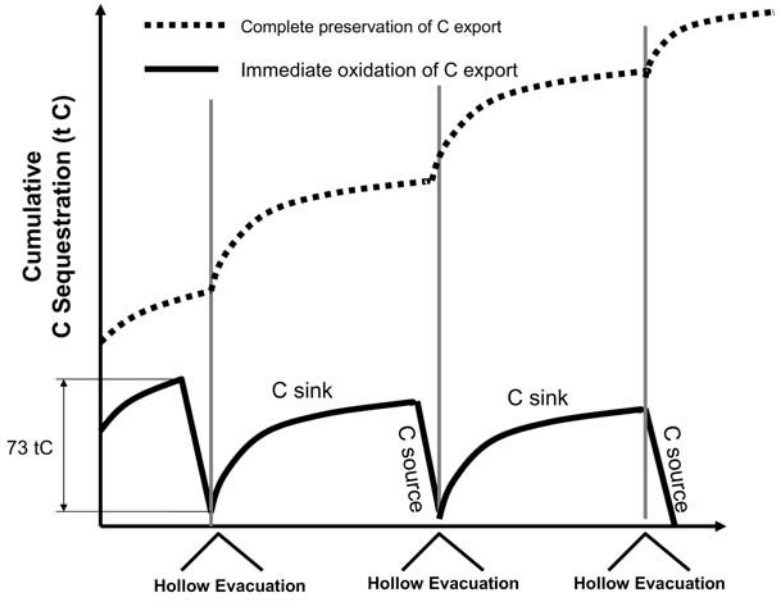

Figure 11. (a) Temporal trends of soil C storage in convex slope, hollows, and the entire watershed, for Tennessee Valley. (b) Two extreme cases of C sequestration by the Tennessee Valley watershed.

SOC accumulation and evacuation in terms of both magnitude and temporal dynamics. This exercise provides implications for the global C cycle at timescales of 10^3 to 10^4 years. The hollow SOC accumulation rate, when divided by the entire watershed, results in a watershed-averaged C accumulation or C sink of 9 kg C m^{-2} during 12 kyr, which is nearly the globally averaged SOC storage of 10 kg C m^{-2} [*Post et al.*, 1982]. This is

equal to the SOC accumulation rate of 0.8 g C m^{-2} yr^{-1}, which is 5–11% of the missing C sink strength for the global land surface of 7.5 to 15 g C m^{-2} yr^{-1} (1–2 Gt C yr^{-1} [*Intergovernmental Panel on Climate Change* (*IPCC*), 2001] divided by the global soil area of 133 $\times$ 10^6 km^2 [*Schlesinger*, 1984]). However, the short-term C sink size or C accumulation rate (slope of SOC storage in Figure 11a) depends on the stage of hollowing infilling as shown earlier in Figure 9b. On level soils not subjected to erosional/depositional processes, the landscape should be at C steady state on these timescales [e.g., *Schlesinger*, 1990]. Below, we discuss the mechanism of this watershed C sink.

5.3. Mechanisms of Hillslope C Sinks

5.3.1. Fate of Eroded Soil Organic Carbon

[46] Less than 10% of annually photosynthesized C is lost via erosion on convex slopes at our two sites. Because the SOC is likely to be at steady state on the convex slope segments (equation (3)), this excess of plant C input over respiration makes the slope a C sink with losses of 1.4 (case I) to 2.7 (case II) g C m^{-2} yr^{-1} at TV, and 5–8 g C m^{-2} at BD. These are significant values compared to the missing C sink strength (7.5 to 15 g C m^{-2} yr^{-1} as calculated above). However, this C sink is meaningful only when it survives oxidation after deposition.

[47] The SOC in depositional areas comes from either (1) soil eroded from upslope areas and/or (2) in situ NPP. We initially hypothesized that eroded SOC would account for much of the hollow SOC. To test this hypothesis, we modeled the TV hollow SOC storage (section 5.1.2) without plant C inputs. The resulting SOC storage, after a 12-kyr model run, was nearly zero due to the high rates of biological decomposition relative to burial. While a total SOC quantity of ~56–120 kg C m^{-2} (180-cm-thick sediment with 2.3–5 C%) was likely deposited during this time period, nearly all of it was oxidized at decomposition rates likely for this area.

[48] This somewhat unexpected conclusion hinges on the selected decomposition rate of the deposited C, which may be more recalcitrant in nature than what we estimated. To address this issue, we used a slower decomposition rate of $0.01 \times e^{-z/13}$ yr^{-1} (e.g., turnover time increasing from 100 years at the soil surface to 1000 years at 30 cm). In this case, 1.7 (eroded soil has 2.3% C) to 2.8 (eroded soil has 5.0% C) kg C m^{-2} survived oxidation, which is still only 7–12% of the total SOC storage measured at H3. This low decomposition rate is unlikely, however. Eroded soil contains C from the A horizons of convex slopes, C that is relatively high in recent plant inputs and labile C components. In annual grasslands in central California, most of the mineral-associated SOC at the surface turns over in less than 100 years [*Baisden et al.*, 2002b]. We anticipate that most of the eroded C from convex slopes at TV is oxidized upon burial, and this negates the apparent C sink caused by erosion on the convex slopes.

5.3.2. In Situ Plant C Inputs and Accumulated Soil Organic Carbon in Hollows

[49] Because eroded C is apparently oxidized in TV hollows, this leaves in situ NPP as the source of accumulated SOC. This is supported by the following analyses. First, the soil sedimentation rate at H3 was multiplied by the C concentration of the sediment (2.3%). The resulting depositional C input is only ~10% of ANPP after ~500–600 years, and eventually declines to the current rate of ~1% of ANPP (Figure 9b). Second, the measured C:N ratios in hollows are significantly higher (meaning the preservation of more labile organic matter) than on the convex slopes (Figure 12a) ($p < 0.001$, ANOVA), suggesting the dominant contribution of in situ NPP (with high C/N ratios) to hollow SOC. In situ NPP also appears to dominate depositional SOC at BD since the depositional C input is currently ~1% of in situ ANPP. However, the difference in C:N ratios between depositional and convex slopes at BD is not as clear as at TV (Figure 12b).

[50] We conclude that the C sink in these watersheds has developed owing to the burial of in situ NPP, rather than the preservation of eroded SOC. We note that there are likely other geomorphic settings where eroding SOC from convex slopes directly enter an area of perennial saturation, leading to more effective retention of eroded SOC. The relative importance of in situ NPP and deposited C on SOC storage in depositional settings is likely to vary greatly with the rates of sediment input, the amount and decomposability of C in the sediment, vegetation types, and microclimates. The fate of eroded SOC in depositional settings is an area deserving of considerable research.

5.3.3. Fate of Soil Organic Carbon Exported From Upland Watershed

[51] The TV watershed continuously and episodically acts as a conveyor of C from the atmosphere to the Earth surface through C export to the downslope fluvial systems. The fate of the exported C greatly affects the atmospheric C. If the C export is immediately oxidized and returns to the atmosphere, the watershed simply repeats cycles of C storage and episodic C release, resulting in no net sink (Figure 11b). However, if there is complete burial of the exported C, a net cumulative sequestration of atmospheric C will occur (Figure 11b).

[52] If the C exported from TV is completely preserved, the long-term (including hollow accumulation and evacuation) geological C sink at TV is 0.8 g C m^{-2} yr^{-1} (Figure 11b). When this rate is extended to an area of 85 $\times$ 10^6 km^2 (the global land with a slope gradient larger than 8% [*Staub and Rosenzweig*, 1992]), this rate would consume the entire atmospheric CO_2 pool within ~10–11 kyr. We know of no indication for such a strong terrestrial sink, and thus a significant fraction of the exported C must be re-oxidized.

[53] The fate of exported C likely varies significantly with space and time. Presently, a significant fraction of exported C may indeed be buried in reservoirs as *Stallard* [1998] has suggested. On geological timescales, oxidation of exported C may also have experienced substantial changes due to the Pleistocene to Holocene sea level changes. The base level variations in many areas must have increased the thickness of floodplain sediments, burying in situ NPP and slowing down the return of C export to the atmosphere. The fate of exported C is presently a poorly constrained question, one that is key

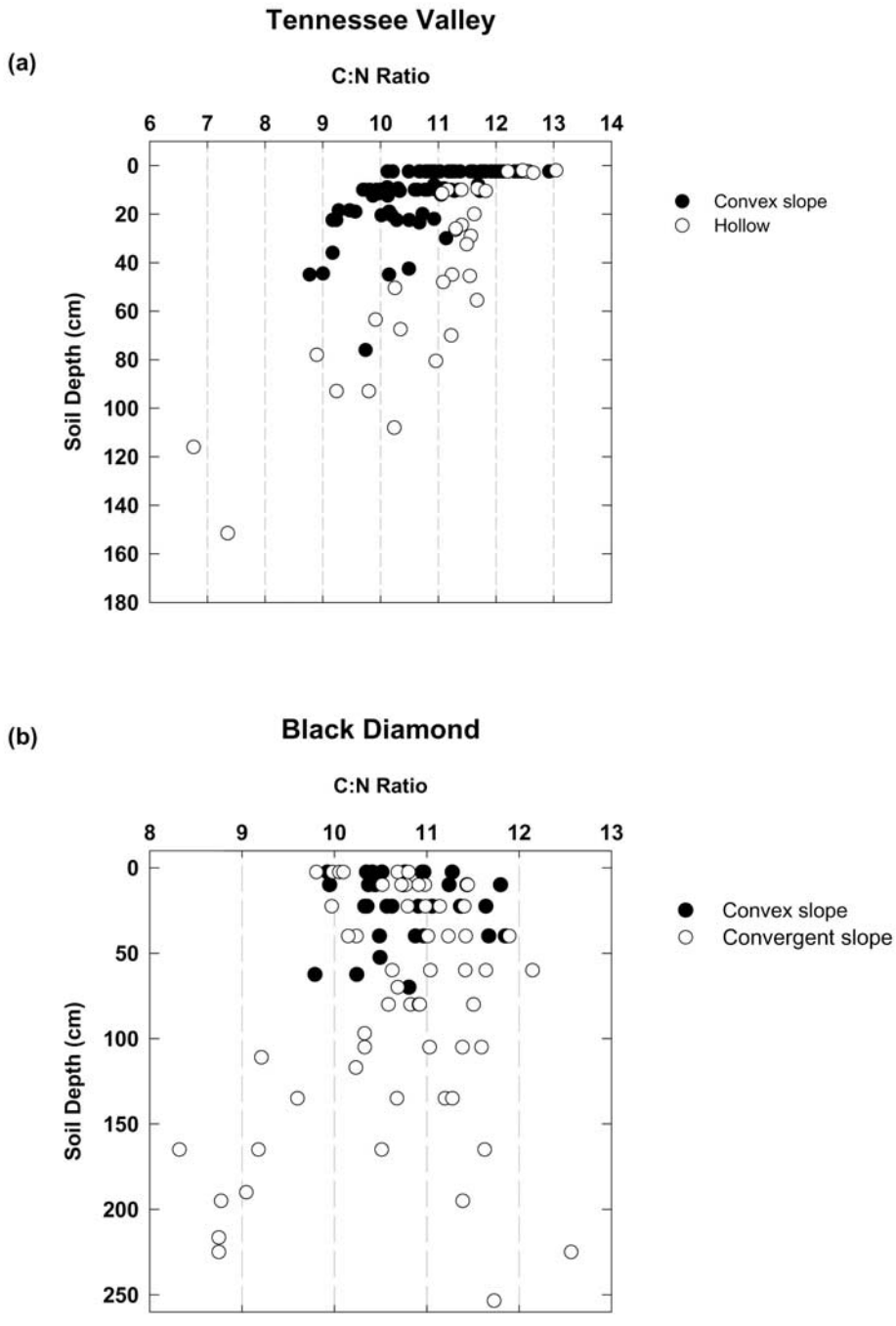

Figure 12. Measured C:N ratios of SOC versus soil depth on convex and convergent slopes. (a) Tennessee Valley. (b) Black Diamond.

to expanding the findings of this study to global spatial scales and to geological timescales.

6. Conclusions

[54] The rates of the erosive removal of C relative to plant inputs on undisturbed convex slopes are, in central California, 10% or less of ANPP, which is, nonetheless, a significant value. On upland soil-mantled hillslopes, much of this eroded C is oxidized upon burial within the watershed. Soil thickening in depositional areas accumulates C mainly from in situ NPP on timescales of 10^3 to 10^4 years. These deposits, in central California and elsewhere, are subject to periodic landsliding and evacuation. Thus soil mantled watersheds are continuous, but stochastically driven, time-dependent C sinks whose importance to global C models is unknown. While undisturbed watersheds lose C at rates much lower than agricultural fields, the sheer area of these

upland landscapes on a global basis make them a significant part of the global C cycle.

[55] Much more information is needed to scale the results from this study conducted on two zero-order watersheds, to the issue of global scale soil-atmosphere C exchange. For example, the magnitude and frequency of mass wasting of the depositional slopes, and their temporal correlations at regional to global scales, have a significant bearing with the dynamics of depositional SOC storage on large spatial scales. Not only the fate of C exported from watersheds, but also the role of exported sediment in creating new soils that bury in situ NPP is deserving of future attention. Additionally, the natural and human-induced changes in fluvial environments may significantly control the decomposition or burial of C exported from the upland hillslopes on different timescales. When combined with soil research, the advancing knowledge on the production, transport, and storage of sediment has much to offer for understanding the C cycle at various scales.

[56] **Acknowledgments.** We thank Aaron Miller, Matt Cover, Cristina Castanha, Jonathan Sanderman, and Stephanie Ewing for their help in field work. This study was funded by the National Science Foundation, the Kearney Foundation of Soil Science, and the Berkeley Academic Senate Committee on Research.

References

Baisden, W. T., R. Amundson, D. L. Brenner, A. C. Cook, C. Kendall, and J. W. Harden (2002a), A multiisotope C and N modeling analysis of soil organic matter turnover and transport as a function of soil depth in a California annual grassland soil chronosequence, *Global Biogeochem. Cycles*, *16*(4), 1135, doi:10.1029/2001GB001823.

Baisden, W. T., R. Amundson, A. C. Cook, and D. L. Brenner (2002b), Turnover and storage of C and N in five density fractions from California annual grassland surface soils, *Global Biogeochem. Cycles*, *16*(4), 1117, doi:10.1029/2001GB001822.

Black, T. A., and D. R. Montgomery (1991), Sediment transport by burrowing mammals, Marin County, California, *Earth Surf. Processes Landforms*, *16*, 163–172.

Culling, W. E. H. (1963), Soil creep and the development of hillside slopes, *J. Geol.*, *71*(2), 127–161.

Day, P. R. (1965), Particle fractionation and particle-size analysis, in *Methods of Soil Analysis 1*, edited by C. A. Black, pp. 545–567, Am. Soc. of Agron., Madison, Wis.

Dietrich, W. E., C. J. Wilson, and S. L. Reneau (1986), Hollows, colluvium, and landslides in soil-mantled landscapes, in *Hillslope Processes: Sixteenth Annual Binghamton Symposia in Geomorphology*, edited by A. D. Abrahams, pp. 361–388, Allen and Unwin, St. Leonard's, NSW, Australia.

Dietrich, W. E., R. Reiss, M. L. Hsu, and D. R. Montgomery (1995), A process-based model for colluvial soil depth and shallow landsliding using digital elevation data, *Hydrol. Proc.*, *9*(3–4), 383–400.

Fernandes, N. F., and W. E. Dietrich (1997), Hillslope evolution by diffusive processes: The timescale for equilibrium adjustments, *Water Resour. Res.*, *33*(6), 1307–1318.

Harden, J. W., J. M. Sharpe, W. J. Parton, D. S. Ojima, T. L. Fries, T. G. Huntington, and S. M. Dabney (1999), Dynamic replacement and loss of soil carbon on eroding cropland, *Global Biogeochem. Cycles*, *13*(4), 885–901.

Harris, D., W. R. Horwáth, and C. V. Kessel (2001), Acid fumigation of soils to remove carbonates prior to total organic carbon or carbon-13 isotopic analysis, *Soil Sci. Soc. Am. J.*, *65*, 1853–1856.

Heimsath, A. M., W. E. Dietrich, K. Nishiizumi, and R. C. Finkel (1997), The soil production function and landscape equilibrium, *Nature*, *388*, 358–361.

Heimsath, A. M., W. E. Dietrich, K. Nishiizumi, and R. C. Finkel (1999), Cosmogenic nuclides, topography, and the spatial variation of soil depth, *Geomorphology*, *27*, 151–172.

Heimsath, A. M., J. Chappell, W. E. Dietrich, K. Nishiizumi, and R. C. Finkel (2000), Soil production on a retreating escarpment in southeastern Australia, *Geology*, *28*(9), 787–790.

Heimsath, A. M., W. E. Dietrich, K. Nishiizumi, and R. C. Finkel (2001), Stochastic processes of soil production and transport: Erosion rates, topographic variation, and cosmogenic nuclides in the Oregon Coast Range, *Earth Surf. Processes Landforms*, *26*, 531–552.

Heimsath, A. M., J. Chappell, N. A. Spooner, and D. G. Questiaux (2002), Creeping soil, *Geology*, *30*(2), 111–114.

Intergovernmental Panel on Climate Change (2001), *Climate Change 2001: The Scientific Basis*, Cambridge Univ. Press, New York.

Jacinthe, P. A., R. Lal, and J. M. Kimble (2001), Organic carbon storage and dynamics in croplands and terrestrial deposits as influenced by subsurface tile drainage, *Soil Sci.*, *166*(5), 322–335.

Jackson, R. B., J. Canadell, J. R. Ehleringer, H. A. Mooney, O. E. Sala, and E. D. Schulze (1996), A global analysis of root distributions for terrestrial biomes, *Oecologia*, *108*, 389–411.

Liu, S., N. Bliss, E. Sundquist, and T. G. Huntington (2003), Modeling carbon dynamics in vegetation and soil under the impact of soil erosion and deposition, *Global Biogeochem. Cycles*, *17*(2), 1074, doi:10.1029/2002GB002010.

Manies, K. L., J. W. Harden, L. Kramer, and W. J. Parton (2001), Carbon dynamics within agricultural and native sites in the loess region of western Iowa, *Global Change Biol.*, *7*, 545–555.

McCarty, G. W., and J. C. Ritchie (2002), Impact of soil movement on carbon sequestration in agricultural ecosystems, *Environ. Pollut.*, *116*, 423–430.

McKean, J. A., W. E. Dietrich, R. C. Finkel, J. R. Southon, and M. W. Caffee (1993), Quantification of soil production and downslope creep rates from cosmogenic ^{10}Be accumulations on a hillslope profile, *Geology*, *21*, 343–346.

Óskarsson, H., O. Arnalds, J. Gudmundsson, and G. Gudbergsson (2004), Organic carbon in Icelandic Andosols: Geographical variation and impact of erosion, *Catena*, *56*(1–3), 225–238.

Page, M., N. Trustrum, H. Brackley, and T. Baisden (2004), Erosion-related soil carbon fluxes in a pastoral steepland catchment, New Zealand, *Agric. Ecosyst. Environ.*, *103*, 561–579.

Post, W. M., W. R. Emanuel, P. J. Zinke, and A. G. Stangenberger (1982), Soil carbon pools and world life zones, *Nature*, *298*, 156–159.

Prosser, I. P., and W. E. Dietrich (1995), Field experiments on erosion by overland flow and their implication for a digital terrain model of channel initiation, *Water Resour. Res.*, *31*(11), 2867–2876.

Prosser, I. P., W. E. Dietrich, and J. Stevenson (1995), Flow resistance and sediment transport by concentrated overland flow in a grassland valley, *Geomorphology*, *13*(1–4), 71–86.

Reichman, O., and E. W. Seabloom (2002), The role of pocket gophers as subterranean ecosystem engineers, *Trends Ecol. Evol.*, *17*, 44–49.

Reneau, S. L., and W. E. Dietrich (1990), Depositional history of hollows on steep hillslopes, coastal Oregon and Washington, *Natl. Geogr. Res.*, *6*, 220–230.

Reneau, S. L., W. E. Dietrich, R. I. Dorn, C. R. Berger, and M. Rubin (1986), Geomorphic and paleoclimatic implications of latest Pleistocene radiocarbon dates from colluvium-mantled hollows, California, *Geology*, *14*, 655–658.

Reneau, S. L., W. E. Dietrich, D. J. Donahue, A. J. T. Jull, and M. Rubin (1990), Late Quaternary history of colluvial deposition and erosion in hollows, central California Coast Range, *Geol. Soc. Am. Bull.*, *102*, 969–982.

Ritchie, J. C., and G. W. McCarty (2003), ^{137}Cesium and soil carbon in a small agricultural watershed, *Soil Tillage Res.*, *69*, 45–51.

Roering, J. J., P. Almond, P. Tonkin, and J. McKean (2002), Soil transport driven by biological processes over millennial timescales, *Geology*, *30*, 1115–1118.

Rosenbloom, N. A., S. C. Doney, and D. S. Schimel (2001), Geomorphic evolution of soil texture and organic matter in eroding landscapes, *Global Biogeochem. Cycles*, *15*, 365–381.

Ruhe, R. V., and P. H. Walker (1968), Hillslope models and soil formation: I. Open systems, *Trans. Int. Congr. Soil Sci.*, *6*(4), 551–560.

Schimel, D., M. A. Stillwell, and R. G. Woodmansee (1985), Biogeochemistry of C, N, and P in a soil catena of the shortgrass steppe, *Ecology*, *66*(1), 276–282.

Schlesinger, W. H. (1984), Soil organic matter: A source of atmospheric CO_2, in *The Role of Terrestrial Vegetation in the Global Carbon Cycle*, edited by G. M. Woodwell, pp. 111–127, John Wiley, Hoboken, N. J.

Schlesinger, W. H. (1990), Evidence from chronosequence studies for a low carbon storage potential of soils, *Nature*, *348*, 232–234.

Smith, S. V., W. H. Renwick, R. W. Buddemeier, and C. J. Crossland (2001), Budgets of soil erosion and deposition for sediments and sedimentary organic carbon across the conterminous United States, *Global Biogeochem. Cycles*, *15*(3), 697–707.

Stallard, R. F. (1998), Terrestrial sedimentation and the carbon cycle: Coupling weathering and erosion to carbon burial, *Global Biogeochem. Cycles*, *12*(2), 231–257.

Starr, G. C., R. Lal, R. Malone, D. Hothem, L. Owens, and J. Kimble (2000), Modeling soil carbon transported by water erosion processes, *Land Degrad. Dev.*, *11*(1), 83–91.

Staub, B., and C. Rosenzweig (1992), Global Zobler soil type, soil texture, surface slope, and other properties: Digital raster data on a 1-degree geographic (lat/long) 180x360 grid, in Global ecosystems database version 2.0, http://dss.ucar.edu/datasets/ds770.0/, NOAA Natl. Geophys. Data Cent., Boulder, Colo.

Trumbore, S. E. (1993), Comparison of carbon dynamics in tropical and temperate soils using radiocarbon measurements, *Global Biogeochem. Cycles*, *7*(2), 275–290.

Trumbore, S. E., J. S. Vogel, and J. R. Southon (1989), AMS ^{14}C measurements of fractionated soil organic matter: An approach to deciphering the soil carbon cycle, *Radiocarbon*, *31*(3), 644–654.

Trumbore, S. E., O. A. Chadwick, and R. Amundson (1996), Rapid exchange between soil carbon and atmospheric carbon dioxide driven by temperature change, *Science*, *272*, 393–396.

Vitousek, P., O. A. Chadwick, P. Matson, S. Allison, L. Derry, L. Kettley, A. Luers, E. Mecking, V. Monastra, and S. Porder (2003), Erosion and the rejuvenation of weathering-derived nutrient supply in an old tropical landscape, *Ecosystems*, *6*, 762–772.

Walling, D. E. (1983), The sediment delivery problem, *J. Hydrol.*, *65*, 209–237.

Yoo, K., R. Amundson, A. M. Heimsath, and W. E. Dietrich (2005), Spatial patterns of soil organic carbon on hillslopes: Integrating geomorphic processes and the biological C cycle, *Geoderma*, in press.

R. Amundson and K. Yoo, Division of Ecosystem Sciences, University of California, Berkeley, 151 Hilgard Hall, Berkeley, CA 94720-3110, USA. (earthy@nature.berkeley.edu; kyoo@nature.berkeley.edu)

W. E. Dietrich, Department of Earth and Planetary Science, University of California, Berkeley, 313 McCone, Berkeley, CA 94720, USA. (bill@geomorph.berkeley.edu)

A. M. Heimsath, Department of Earth Sciences, Dartmouth College, 6105 Fairchild Hall, Hanover, NH 08755, USA. (arjun.heimsath@dartmouth.edu)

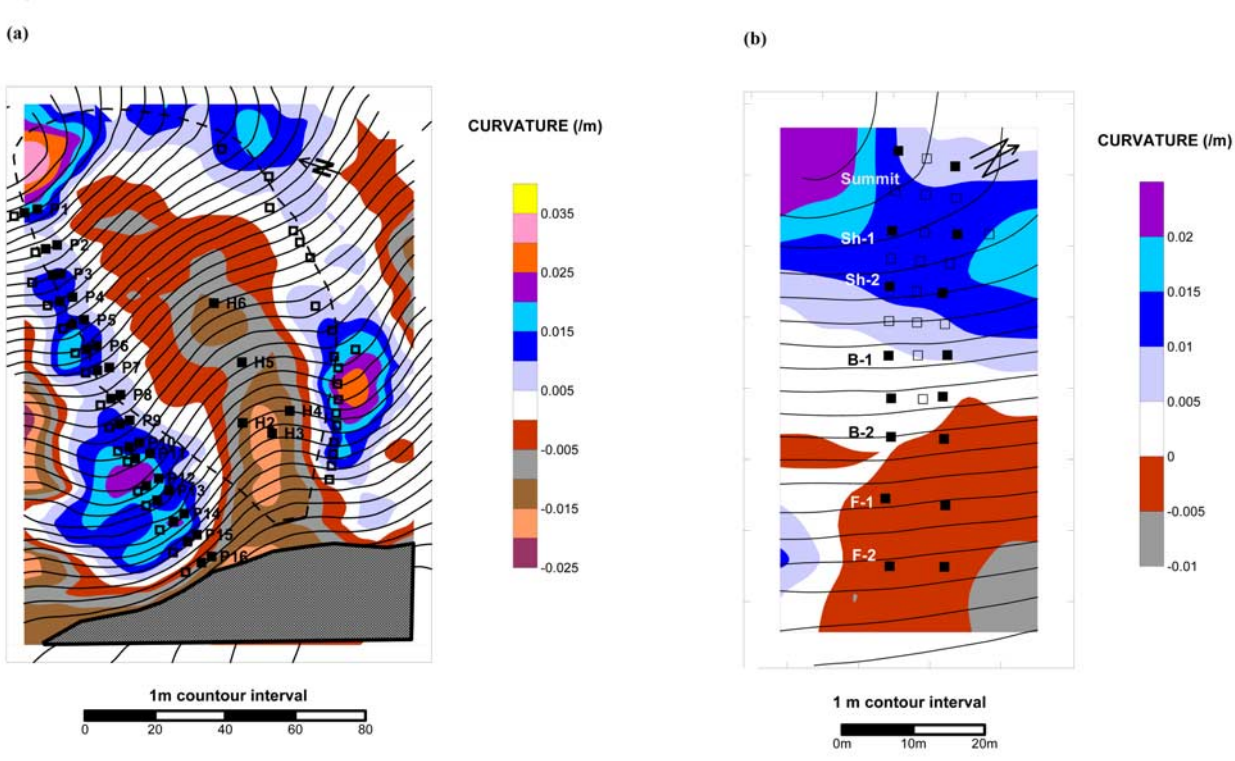

Figure 2. Map of study sites. (a) Tennessee Valley and (b) Black Diamond. The solid squares represent soil pits where samples were taken. The open squares represent sites where only soil thicknesses were measured. The dashed line at TV defines the boundary of the zero-order watershed.

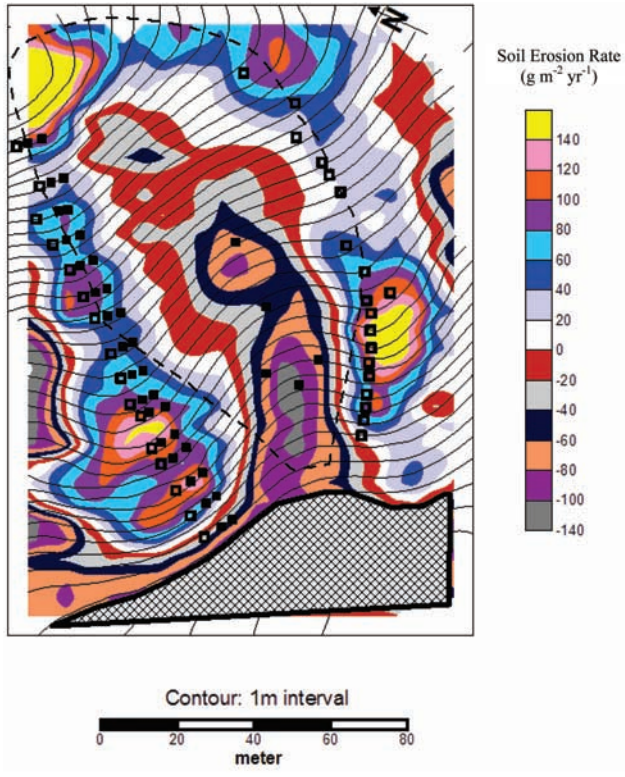

Figure 4. Calculated soil erosion rates at Tennessee Valley. A negative quantity indicates deposition. The floodplain (hatched area) is not included in the calculation.

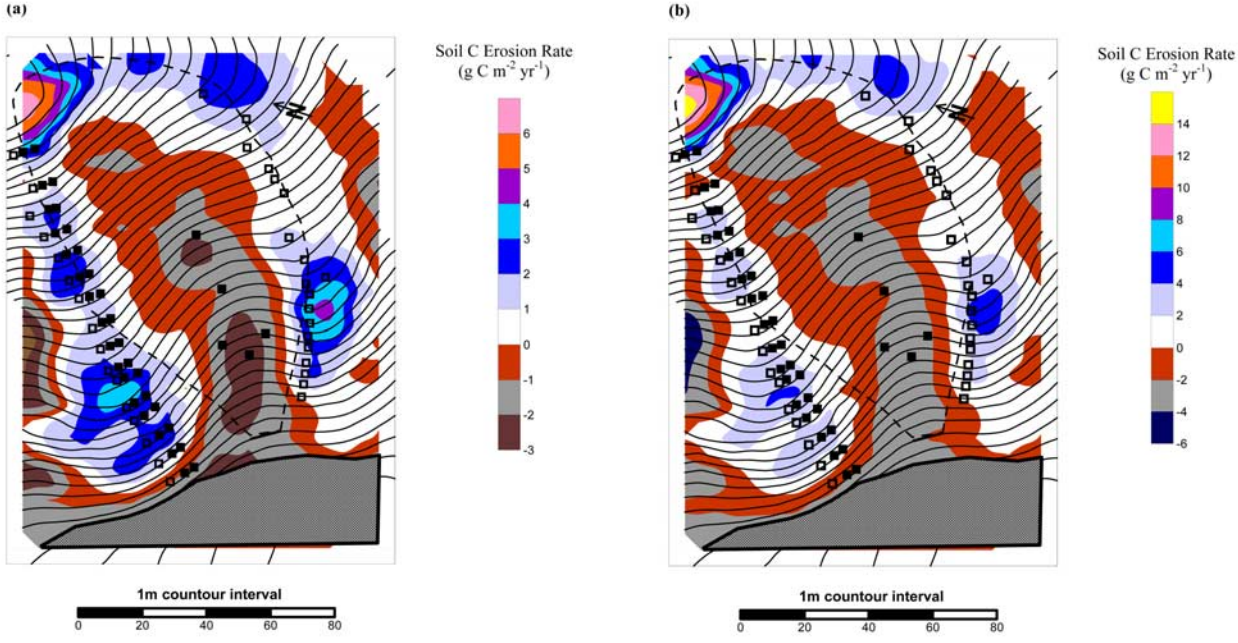

Figure 6. SOC erosion loss at Tennessee Valley. (a) Case I. (b) Case II. Negative quantities indicate deposition. The floodplain (hatched area) is not included in the calculation.